Journal of JSEM, Vol.10, Special Issue (2010) 199-204

Microchanneling and Lining Layer Formation by Spontaneous Infiltration in Fe-Cu System

Takuhiro KODAMA[1], Tatsuya OHMI[1] and Manabu IGUCHI[1]

[1] Graduate School of Engineering, Hokkaido University, Sapporo, Japan

(*Received 31 January 2010; received in revised form 31 May 2010; accepted 12 June 2010*)

Abstract

The influence of the body-metal powder size on the microchanneling behavior and the lining-layer formation in the powder-metallurgical microchanneling process was investigated using the combination of iron powder and copper wire. Iron powders 45 μm and 110 μm in average diameters were examined. Open microchannels and clear lining layers were formed in all specimens. The coarser iron powder tended to reduce the homogenization rate of the composition of the lining layer.

Key words

Microchannel, Powder Metallurgy, Diffusion, Copper, Iron

1. Introduction

In these years, microreactor technology has attracted more and more attention.[1] Microreactors have high reaction efficiency and contribute to the saving of the processing time and the raw materials. Metallic materials have good thermal conductivity, high heat resistance, and excellent formability. Therefore, metallic microreactors are suitable for high-temperature catalytic reactions, such as synthesis and steam reforming of methanol [2-4]. The microreactors contribute to settle the environmental problems by improving efficiency of these reactions.

In general, microchannels with characteristic dimension of several tens or several hundreds micrometers are used as the reaction space in the microreactors. Some microchanneling processes have been used: precision mechanical machining [5], photoetching, micro-electro discharge machining, laser or electron beam machining, and galvanization. With these processes, however, many steps are required to construct the microreactors, and the fabrication of microchannels with three-dimensional shapes is difficult to produce.

We proposed a powder-metallurgical microchanneling process which was able to produce arbitrarily-shaped microchannels with a simple operation.[6, 7] Figure 1 shows the concept of the process. In this process, a combination of two kinds of metals with different melting points is used. One is the body metal which has higher melting point and is to make up the body of the microchannel device, and the other is the sacrificial-core metal which gives the shape of the microchannel. A body metal powder and shaped sacrificial-core metal are compressed, and the resulted compact specimen is then sintered. During heating of the specimen, the sacrificial-core metal melts and migrates to the body metal region by infiltration and diffusion. The migration of the molten sacrificial-core metal causes the formation of the microchannel. In addition, an alloy layer lining the microchannel is often produced simultaneously.

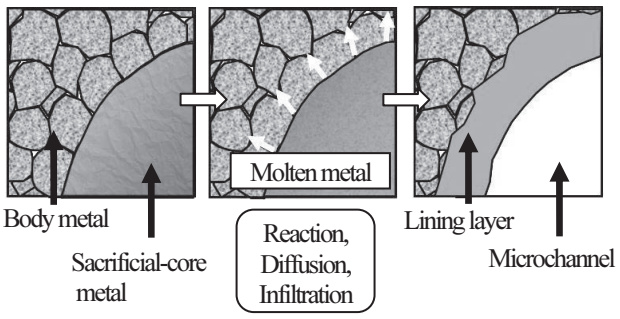

Fig. 1 Schematic illustration of the concept of the powder-metallurgical microchanneling process

In this process, the shape of the microchannel and the structure of the lining layer change depending on the combination of the metals. Figure 2(a) presents a back-scattered electron image near the site initially occupied by the sacrificial core in a specimen produced from iron (body metal) and copper (sacrificial-core metal), hereinafter designated as Fe/Cu. Figure 2(b) shows that in a Ni/Cu specimen. When the body metal was iron, both the microchannel and the lining layer were formed. On the other hand, no microchannel was formed in the case of nickel. According to our previous researches, various factors, such as the size of the body-metal powder, the pressing pressure for the green compact, the sintering conditions and the shape of the sacrificial core, affect the formation of microchannels and lining layers in a complex way. This aspect was, however, based on the observation of the structures after sintering, and thus sequences of microchanneling and lining-layer formation have not yet been known sufficiently.

The ultimate goal of our researches about this process is precise prediction and control of the shape of the microchannel and the properties of the lining layer in an arbitrary combination of the body metal and the sacrificial-core metal.

Recently, we have researched the formation mechanism of the microchannels in the Fe/Cu specimen using an iron powder 45 μm in diameter.[9] Figure 3 shows the structure in the Fe/Cu specimen quenched at 1358 K, the melting point of copper. Figures 3(a) and (b) depict different cross sections of the same specimen. In Fig. 3(a), the sacrificial core still remained at the initial site, probably because this portion was solid, or liquid but quenched just before the full-scale infiltration. In Fig. 3(b), on the other hand, a cavity had already formed. This indicates that the molten copper infiltrates into the iron powder region immediately after melting, and thus produces the microchannel. After the rapid infiltration, the distribution of copper in the lining layer was uniformed by diffusion during sintering.

Figure 4 shows a Cu-side portion of the Fe-Cu binary alloy phase diagram. The Cu-side liquidus and solidus lines of the Ni-Cu system are also illustrated in this figure. The equilibrium solid phases near the melting point of Cu in the Fe-Cu system are Cu-based solid solution and γ-Fe solid solution. In the Ni-Cu system, the equilibrium solid phase at high temperatures is one Ni-Cu solid solution with complete solubility. No intermetallic compound forms in each system. The distribution coefficients near the melting point of Cu are 1.3 and 1.4 in the Fe-Cu and Ni-Cu systems, respectively. Thus, the phase relations were similar in both systems just after melting of Cu. This indicates that the marked difference in the microchanneling behavior between these systems in Fig. 2 was related not to the phase relations but mainly to the capillarity effect.

The size of the body-metal powder influences the geometry of the infiltration pathways for the molten sacrificial-core metal. Therefore the infiltration behavior and the homogenization rate of the sacrificial-core metal in the lining layer may be influenced.

In this study, we examined the influence of iron powder size on the microchanneling behavior and the lining layer formation in the Fe/Cu specimen by using two kinds of iron powders 45 and 110 μm in diameters.

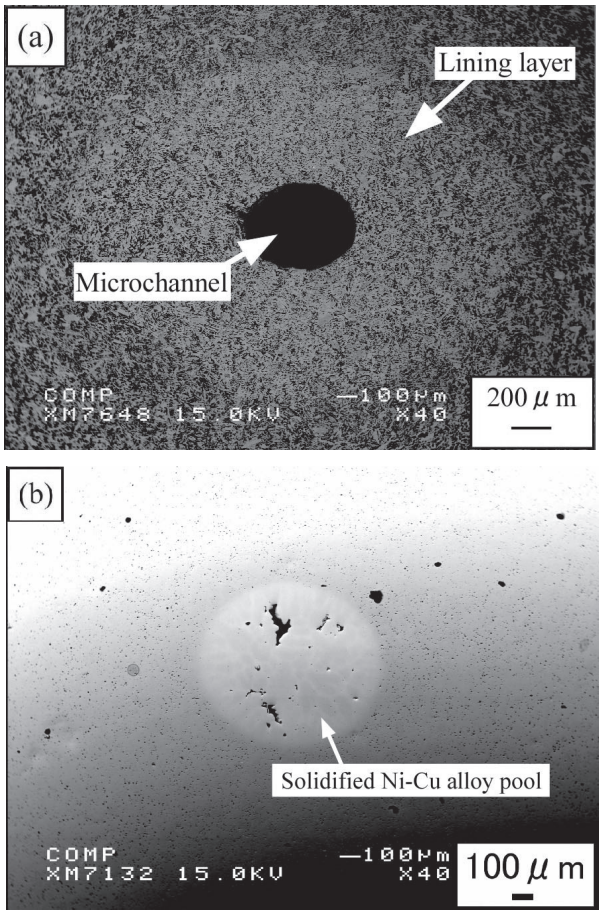

Fig. 2 Back-scattered electron images near the sites initially occupied by the sacrificial cores. (a) Fe/Cu. (b) Ni/Cu [8]. Diameter of each sacrificial core (d_s) was 500 μm. The compacting pressure was 530 MPa

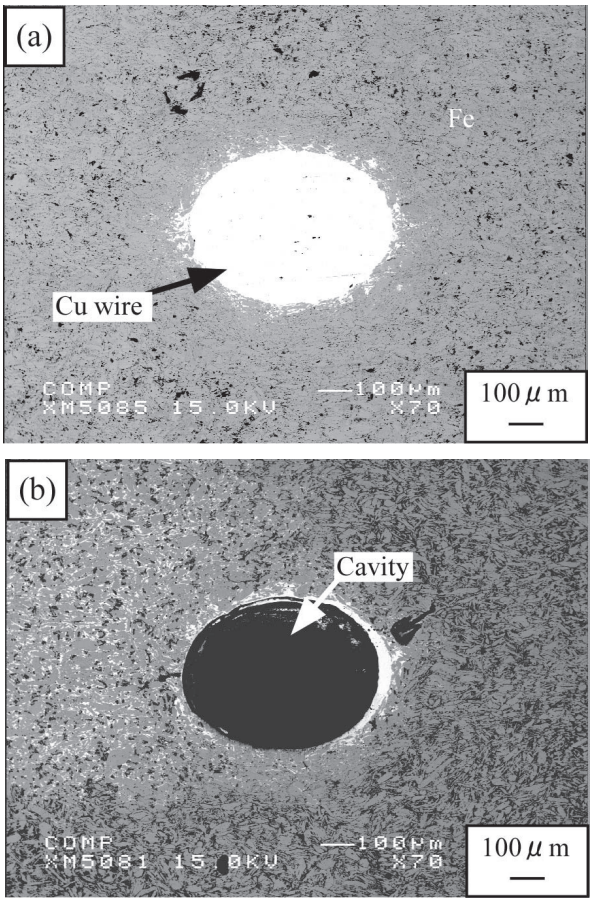

Fig. 3 Back-scattered electron images near the sites initially occupied by the sacrificial cores in the Fe/Cu specimen quenched at 1358 K.[9] Diameter of the sacrificial core was 500 μm. Photographs (a) and (b) show different cross sections of same specimen

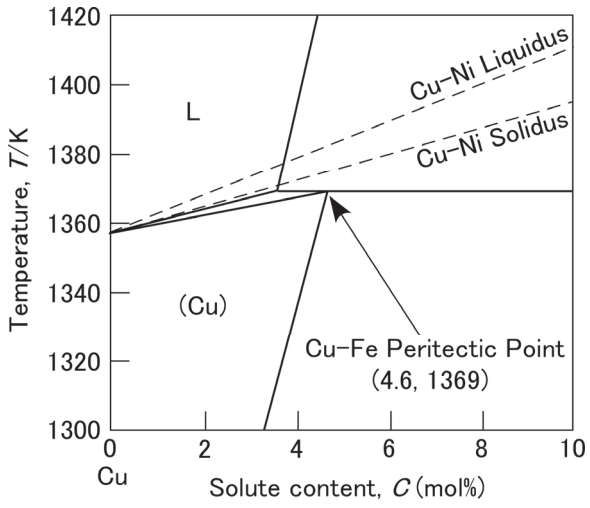

Fig. 4 Cu-side portion of the Fe-Cu binary alloy phase diagram with the liquidus and solidus lines of the Ni-Cu system based on the binary alloy phase diagrams edited by Massalski [10]

2. Experimental Procedure

An iron powder 45 μm or 110 μm in average diameter and a copper wire with a diameter of 500 μm were compressed uniaxially under a given pressure: 155, 230, 305, 380, 455, 530, 605, 680, or 755 MPa.

The compacted specimen was heated at 0.2 K/s, in an argon gas atmosphere, and then, quenched at a prescribed temperature, 1358, 1363, 1373, 1423, or 1473 K, by soaking in a Wood's metal bath. For comparison, some specimens were furnace-cooled at 0.4 K/s from 1473 K. The maximum temperature, 1473 K, is 115 K higher than the melting point of copper. The heat-treated specimen was then cut across or along the microchannel.

3. Results and Discussion

3.1 Microchanneling behavior

Figure 5 describes the relationship between the compacting pressure, *P*, and the porosity of the green compact, *E*, in both cases of 45 and 110 μm-diameter powders. The coarser iron powder was easily compressed. Therefore, the porosity of the green compact was lower in the case of 110 μm-diameter powder than the other compacted under the same pressure. Figure 6 shows an example of the structure near the microchannel produced using the 110 μm-diameter powder. The specimen was furnace-cooled at 1473 K. In this study, the microchannels were open throughout the entire length in all specimens.

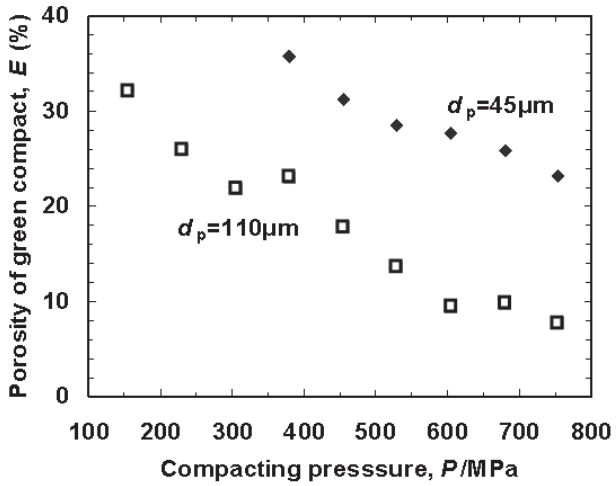

Fig. 5 Relationship between the compacting pressure, *P*, and the porosity of the green compact, *E*. d_p is the average diameter of the iron powder particles

3.2 Infiltration and diffusion of copper in the lining layers

Figures 7(a) and (b) show magnified photographs of the structures in the lining layers. They compare the influence of the iron-powder size on the lining-layer structure quenched at 1363 K, which is 5 K higher than the melting point of the copper. In both specimens, the clear-white region between the iron particles corresponds to a copper-rich phase, whose copper concentration was about 90 mol%. This yields the primary evidence for the infiltration of the molten copper into the compacted iron-powder region. The light gray region is a supersaturated iron solid solution containing copper diffused from neighboring copper-rich regions. It's worth noting that the copper-rich phase seems to have infiltrated preferably via narrow pathway as typically seen in Fig. 7(b). This result indicates that the wettability of the molten copper to the solid iron is very good, and explains the fact that the open microchannels were produced even in the low-porosity specimens. In this regard, the Fe-Cu system is quite different from the Ni-Al system in which the formation processes of the microchannel and the lining layer varied greatly depending on the green-compact porosity. In the Ni-Al system, typical reactive infiltration occurred only in the case when the green-compact porosity, *E*, was high, for example, *E*= 36.0%.[11] When the porosity was 31.5% or lower, on the other hand, a porous intermetallic lining layer controlled the migration of the sacrificial-core metal.[11]

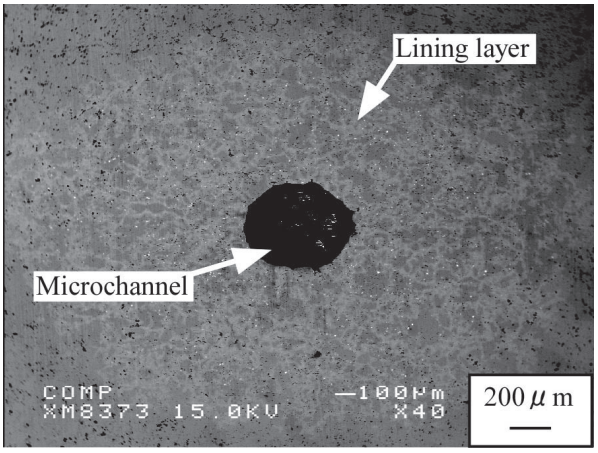

Fig. 6 Back-scattered electron image near the microchannel in the Fe/Cu specimen furnace-cooled from 1473 K. The average diameter of the iron powder was 110 μm, and the porosity of the compact specimen, *E*, was 13.6%

Table 1 lists the area ratio of the copper-rich region in the lining layer, *Γ*, and the value of *Γ*/*E* for each specimen shown in Fig. 7. The values of *Γ* were measured by image analysis of the back-scattered electron images of the lining layers. The results indicate that about 18% of the pore space in the powder-compact region acted as the infiltration pathways in the specimen made from 45 μm-diameter powder. Meanwhile, the ratio of the infiltration pathways in the case of 110 μm-diameter powder was approximately half of the other. This is probably because the compacted coarse powder had a lot of large pores that could persist during infiltration of the molten copper.

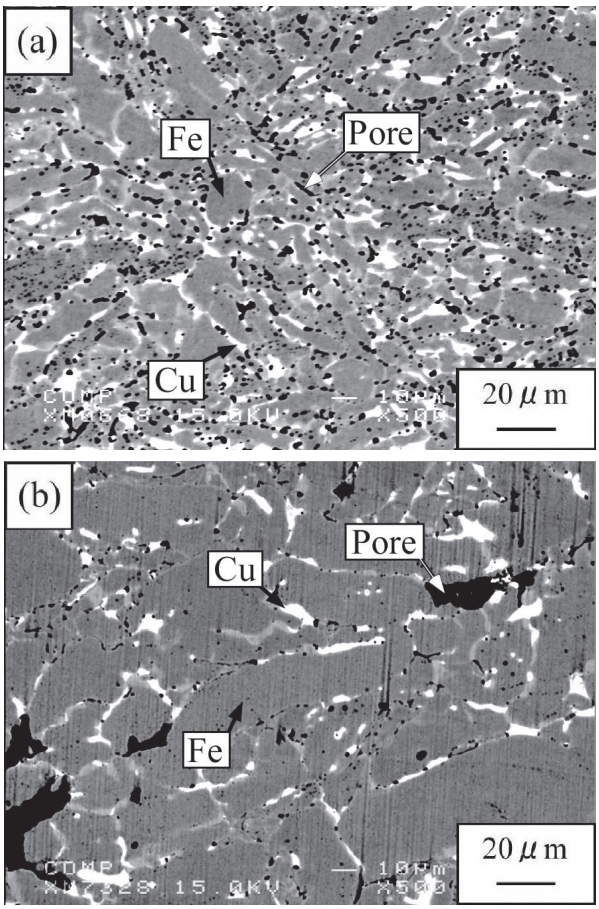

Fig. 7 Magnified photographs of the structures of the lining layers in the specimens quenched at 1363 K. The average diameters of the iron powders were 45 μm (a) and 110 μm (b). The green-compact porosity in each specimen was 32.0 ± 0.7 (%)

Table 1 Parameters for the characterization of the infiltration behavior in the lining layers shown in Figs. 6(a) and (b). Γ is the area ratio of the copper-rich phase

Parameters	d_p / μm	
	45	110
Γ	5.8 %	2.5 %
Γ / E	0.18	0.08

Figure 8 shows the structure of the specimen quenched at 1363 K and the copper concentration profile across the lining layer. In Fig. 7(b), there are many sharp peaks of the copper concentration. These peaks correspond to the copper-rich regions distributed in the lining layer. Figure 9 presents the EPMA result of the furnace-cooled specimen. The copper-concentration peaks observed at 1363 K disappeared and the composition was homogenized as shown in Fig. 9(b). This result shows that after the rapid infiltration of molten copper, diffusion of copper progressed in the lining layer with increases of the heating time and temperature.

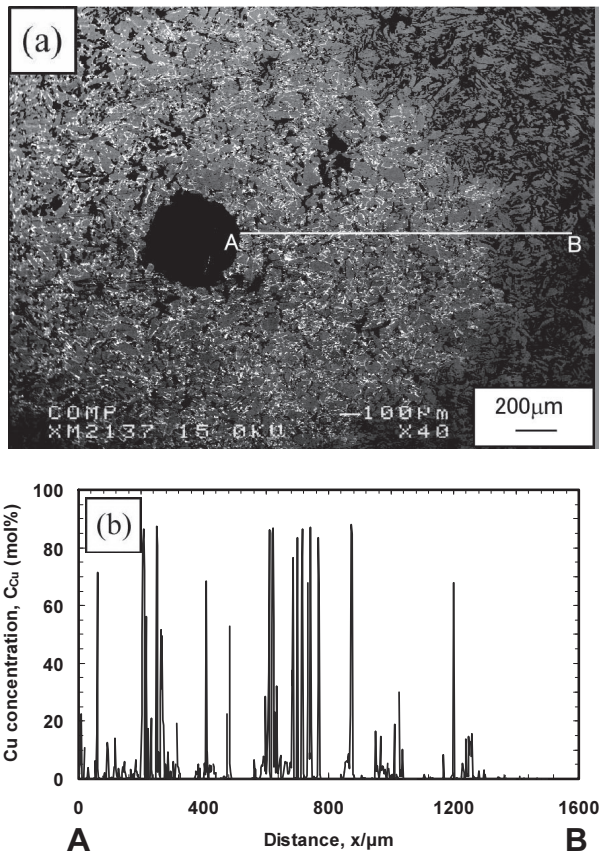

Fig. 8 Back-scattered electron image (a) and copper-concentration profile (b) near the microchannel in the specimen quenched at 1363 K. The average diameter of the iron powder was 110μm. Porosity of the green compact, E, was 32.2%

Figure 10 describes the lining-layer structures in the specimens furnace-cooled from 1473 K. In the case of the 45 μm-diameter powder (Fig. 10(a)), most of the white copper-rich regions had already vanished with diffusion of copper. In Fig. 10(b), on the other hand, the white spots still remained. This is because the size of the pore space in the green compact increases as the powder particle size increases.

Table 2 lists the arithmetical mean deviation of the concentration profile, R_c, which is an effective index of the unevenness of the concentration profile,[9] R_c was calculated according to the following expression:

$$R_c=(1/L)\int_0^L |f(x)|\mathrm{d}x$$

where x and L are the distance from the inner wall of the microchannel and the regulation length, respectively. $|f(x)|$ is the absolute difference between the concentration at the position $x = x$, c_x, and the average concentration, c_{av}. This time, dx was 2 μm, and the ratio of L divided by d_p was set at 6.67. Diameter of the electron beam for the EPMA was 1 μm. Table 2 presents the values of R_c derived from copper concentration profiles measured across the lining layers in various specimens. The porosity of the green

compact, E, for each specimen was in the range from 31 to 32 (%). In both cases of 45 μm- and 110 μm-diameter powders, the value of R_c was decreased monotonically with increases of the heating time and temperature. That is to say, this result confirms that R_c is an available parameter on evaluation of the rate of the concentration homogenization. It is worthy of remark that the difference of mean diameters of the body-metal powder caused a significant difference on the value of R_c of the furnace-cooled specimens. The higher R_c value of the furnace-cooled specimen when d_p= 110 μm represents the survival of more copper-rich regions during sintering. This result consists with the structural feature of the lining layer shown in Fig. 7(b).

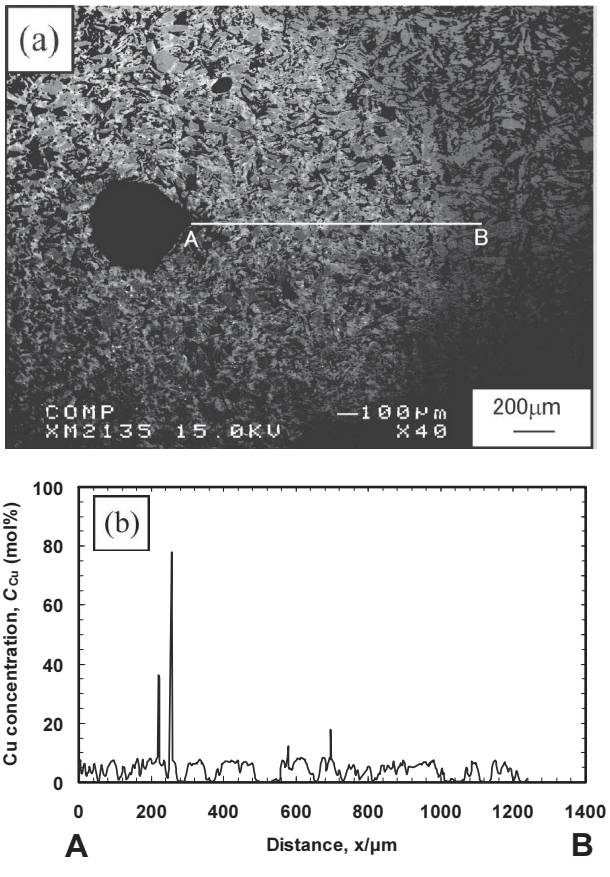

Fig. 9 Back-scattered electron image (a) and copper-concentration profile (b) near the microchannel in the furnace-cooled specimen. The average diameter of the iron powder was 110 μm. E = 32.1%

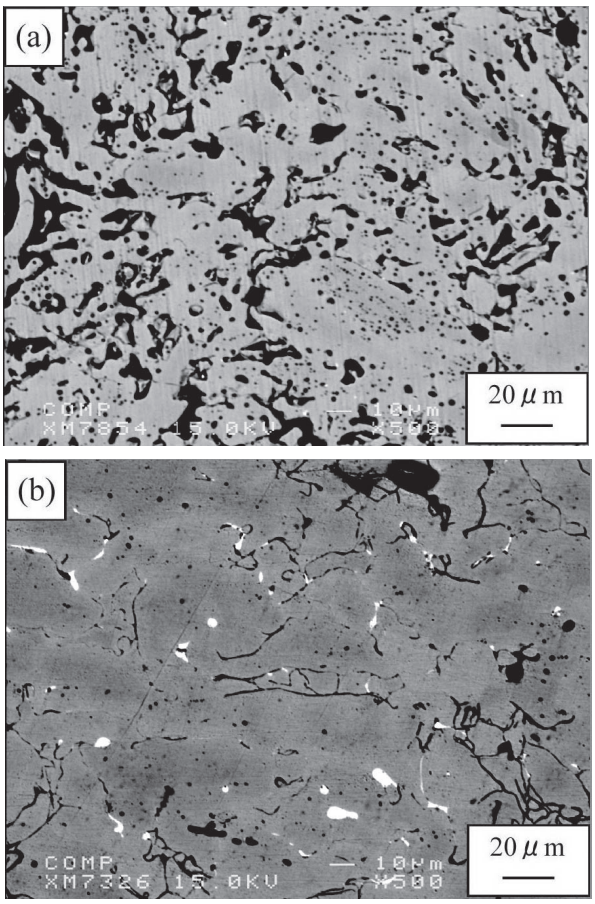

Fig. 10 Magnified photographs of the structures of the lining layers in the specimens furnace-cooled from 1473 K. The average diameters of the iron powders were 45 μm (a) and 110 μm (b)

Table 2 Influence of average diameter of the body-metal powder, d_p, on the arithmetical mean deviation of the concentration profile, R_c

Specimen	R_c (mol%)	
	d_p= 45 μm [9]	d_p= 110 μm
Q(1363K)	9.86	10.06
Q(1423K)	7.24	6.93
Q(1473K)	2.91	3.61
FC(1473K)	0.97	2.83

Q: Quenched, FC: Furnace–cooled

4. Conclusions

We investigated the influence of the iron powder size on the microchanneling behavior and the lining-layer formation in the Fe/Cu specimens. The results of our research are summarized as follows.

1. Open microchannels and lining layers were produced in all specimens.
2. The ratio of the infiltration pathways to the initial pore space is higher in the case of the 45 μm-diameter powder than in the case of the 110 μm-diameter powder.
3. Homogenization of the composition in the lining layer retarded in the case of coarse iron powder.

References

[1] Rebrov, E. V., de Croon, M.H.J.M. and Schouten, J. C.: Design of a microstructured reactor with integrated heat-exchanger for optimum performance of a highly exothermic reaction, *Catalysts Today*, **69** (2001), 183-192.

[2] Zapf, R., Becker-Willinger, C., Berresheim, K., Bolz, H., Gnaser, H., Hessel, V., Kolb, G., Löb, P., Pannwitt, A.-K. and Ziogas, A.: Detailed Characterization of Various Porous Alumina-Based Catalyst Coatings Within Microchannels and Their Testing for Methanol Steam Reforming, *Trans IChemE*, **81** (2003), 721-729.

[3] Aartun, I., Silberova, B., Venvik, H., Pferfer, P., Görke, O., Schubert, K. and Holmen, A.: Hydrogen production from propane in Rh-impregnated metallic microchannel reactors and alumina foams, *Catalysis Today*, **105** (2005), 469-478.

[4] Pfeifer, P., Schubert, K., Liauw, M.A. and Emig, G.: PdZn catalysts prepared by washcoating microstructured reactors, *Applied Catalysis A: General*, **270** (2004), 165-175.

[5] Papautsky, I., Frazier, A.B. and Swerdlow, H.: A Low-Temperature IC-Compatible Process for Fabricating Surface-Micromachined Metallic Microchannels, *Journal of MEMS*, **7** (1998), 267-273

[6] Ohmi, T., Sakurai, M., Matsuura, K. and Kudoh, M.: Formation of Microchannels in Sintered Titanium-Powder Compacts by Local Reactive Infiltration, *Proceedings of the 15th International Symposium on Transport Phenomena*, (2004), 364-367.

[7] Ohmi, T., Takatoo, M., Iguchi, M., Matsuura, K. and Kudoh, M.: Powder-Metallurgical Process for Producing Metallic Microchannel Devices, *Mater. Trans*., **47** (2006), 2137-2142.

[8] Sato, M., Ohmi, T., Iguchi, M. and Matsuura, K.: Influence of Kinds of Base Metal and Sacrificial-Core Metal on Microchannel Formation in Metallic Sintered Compacts, *Functionally Graded Materials*, **20** (2006), 134-139.

[9] Ohmi, T., Kodama, T. and Iguchi, M.: Formation Mechanism of Microchannels and Lining Layers in Sintered Iron Powder Compacts with Copper Sacrificial Cores, *Materials Transactions*, **50** (2009), 2891-2896.

[10] Massalski T. D.: Binary Alloy Phase Diagrams. Second Edition Plus Updates on CD-ROM, (ASM International, Metal Park, Ohio, 1996).

[11] Ohmi, T., Hayashi, N. and Iguchi, M.: Formation of Porous Intermetallic Thick Film by Ni-Al Microscopic Reactive Infiltration, *Materials Transactions*, **49** (2008), 2723-2727.